INNER HELIOSPHERIC FLUX ROPE EVOLUTION VIA IMAGING OF CORONAL MASS EJECTIONS

T. A. HOWARD AND C. E. DEFOREST

Southwest Research Institute, 1050 Walnut Street, Suite 300, Boulder, CO 80302, USA

ABSTRACT

Understanding the evolution of flux ropes in coronal mass ejections (CMEs) is of importance both to the scientific and technological communities. Scientifically their presence is critical to models describing CME launch and they likely play a role in CME evolution. Technologically they are the major contributor to severe geomagnetic storms. Using a new processing technique on the *STEREO*/SECCHI heliospheric imaging data, we have tracked a magnetic flux rope observed by the *Wind* spacecraft in December 2008 to its origins observed by coronagraphs. We thereby establish that the cavity in the classic three-part coronagraph CME is the feature that becomes the magnetic cloud. This implies that the bright material ahead of the cavity is piled-up coronal or solar wind material. We track the evolution of the cavity en-route and find that its structure transforms from concave inward (curving away from the Sun) to concave outward (toward the Sun) around 0.065 AU from the Sun. The pileup was tracked and its leading edge remained concave inward throughout its journey. Two other CMEs in January 2009 are also inspected and a similar cavity is observed in each, suggesting that they too each contained a flux rope. The results presented here are the first direct observation, through continuous tracking, associating a particular flux rope observed in situ with the same flux rope before ejection from the corona. We speculate that detailed heliospheric imagery of CMEs may lead to a means by which flux ropes can be identified remotely in the heliosphere.

Key words: interplanetary medium – methods: data analysis – solar-terrestrial relations – Sun: coronal mass ejections (CMEs) – Sun: heliosphere – Sun: magnetic topology

Online-only material: animations, color figures

1. INTRODUCTION

Since the first identification of magnetic clouds in the early 1980s (Burlaga et al. 1981; Klein & Burlaga 1982), magnetic flux ropes have long been known to be present within coronal mass ejections (CMEs). In simple terms, a flux rope is a collection of magnetic field lines that group together to form a large structure, and in the case of magnetic clouds this structure is of a tightly wound spiral. The origin of this structure is believed to be at or near the Sun with the "winding up" and/or shearing of field lines prior to the CME launch. Many models describing the onset and early evolution of CMEs rely on the presence or establishment of a magnetic flux rope (e.g., Martin et al. 1985; Sturrock 1989; van Ballegooijen & Martens 1989; Török, & Kliem 2003, 2005; Fan & Gibson 2003a; Fan 2005), and it is generally accepted that magnetic clouds cause large magnetic storms at the Earth (e.g. Wilson 1990; Marubashi 2000; Echer et al. 2005). It is hence of interest to both the scientific and technological communities to understand the nature of flux rope evolution through the heliosphere, particularly those within CMEs.

The nature of magnetic clouds near 1 AU is very well known with multiple studies of their anatomy and nature studied via in situ measurements (e.g., Klein & Burlaga 1982; Gloeckler et al. 1999; Lepri et al. 2001; Lynch et al. 2003; Cane & Richardson 2003; Richardson & Cane 2004). Magnetic clouds are widely believed to be flux ropes, and many models have been devised that attempt their reconstruction using magnetic field and plasma density observations obtained by in situ spacecraft. These can be divided into two classes: force-free (Burlaga 1988; Lepping et al. 1990; Hidalgo et al. 2000); and non-force-free (Hu & Sonnerup 2001; Hasegawa et al. 2004; Liu et al. 2007). Riley et al. (2004) review the performance of many of these techniques.

Near the Sun, the absence of in situ data has left only speculation as to the presence and appearance of flux ropes within CMEs as observed with coronagraphs. Unlike the high level of spiral structure observed in posteruptive arcades (e.g., Tripathi et al. 2004) or the so-called sigmoid structures that are highly suggestive of flux ropes (e.g., Canfield et al. 1999; McKenzie & Canfield 2008) lower in the corona, structures observed in the higher corona are much less distinguished, and observational evidence has been lacking to establish exactly where in the coronagraph CME the flux rope lies. For the purposes of simplicity, we will confine our discussion to those CMEs displaying the so-called classic three-part structure.

The classic three-part CME, first identified using *Solar Maximum Mission* C/P observations (Illing & Hundhausen 1985), consists of a leading bright front, followed by a dark cavity, followed by a bright core. An example of an image of such a CME can be sought from the NASA *Solar and Heliospheric Observatory* Web site (at http://soho.nascom.nasa.gov/hotshots/2000_02_26/). Variations on this theme can be significant in geometry and intensity, but this basic structure exists for a large proportion of coronagraph CMEs. It is accepted that the innermost section of the three parts, the filament of the "light-bulb" structure, is also the filament (or prominence) observed as an eruption in X-ray, EUV, UV, or Hα imagers. This has been confirmed irrefutably using *STEREO* images from the Extreme Ultra-Violet Imager (EUVI) and COR1 (see the *STEREO* Web site at http://stereo.gsfc.nasa.gov/ for examples of the tracking of filaments within erupting CME structures). It is also generally assumed (e.g., Forsyth et al. 2006) that the cavity component evolves to become the in situ magnetic cloud, and its decreased intensity as seen by coronagraphs is maintained at least until it is observed by in situ spacecraft near 1 AU. While a reduction in density is not one of the three signatures of a magnetic cloud (Burlaga et al. 1981), many, but not all, magnetic clouds

observed in situ do have a density that is lower than their surroundings. This is believed to arise from elevated magnetic pressure that acts to evacuate the density within the flux rope (Chen et al. 1997). Theoretical work involving the development of cavities includes Fuller et al. (2008).

While it has been widely suspected that the in situ manifestation of the classic CME is that the sheath is the leading bright front and the magnetic cloud is the cavity, this has never before been confirmed observationally. Observational confirmation can be established if we are able to track CME features continuously from the Sun out to 1 AU and can then compare directly with data from in situ spacecraft there. These are two of the promises of the *STEREO*/SECCHI mission, and a newly developed pipeline for the outermost SECCHI heliospheric imager now makes this a reality. In this report, we present results tracking three CMEs continuously from the Sun to 1 AU using the SECCHI imaging suite on *STEREO*. One of these is a well-documented CME that passed an in situ spacecraft at Earth and *STEREO B* where a magnetic cloud was observed. We track the magnetic cloud through SECCHI to its coronagraph origins and establish that it is indeed the cavity that becomes the in situ magnetic cloud. An analysis of the structure and evolution of the cavity and leading sheath follows, and we conclude with a discussion on the implications for future CME observations.

2. METHODOLOGY

Data analysis in this reported study can be divided into two stages: data processing, which provided the cleaned images; and data analysis, which includes the three-dimensional reconstruction efforts. These are described in the following sections, which include a discussion of the instruments used, the studied events, and the terminology adopted.

2.1. Data and Processing

The primary data set utilized for this study is SECCHI on board *STEREO A*. *STEREO* (Kaiser et al. 2008) is a pair of identical spacecraft launched in 2006 October into solar-ecliptic orbit. Their orbits are designed such that their angular separation from the Sun–Earth line increases by approximately 22°.5 each year, with *STEREO A* leading and *STEREO B* lagging the Earth. At the time of the observations in the present study (2008 December–2009 January), *STEREO A* was ∼43° west of the Sun–Earth line (right when looking at the Sun from the Earth) and *STEREO B* was ∼46° east (left).

The SECCHI instrument suite (Howard et al. 2008) consists of five imagers on each *STEREO* spacecraft. They are designed such that their fields of view overlap, so a continuous view of the solar wind from the Sun through 90° elongation can be accomplished. Moving from the Sun outward EUVI images the whole disk Sun in EUV and the coronagraphs COR1 and COR2 observe from 1.3 to 4.0 $R_\odot$ and 2.5 to 15.0 $R_\odot$, respectively, with full position angle (PA) coverage.

To observe the outer regions of the inner heliosphere, SECCHI has two heliospheric imagers (Eyles et al. 2009). HI-1 observes from 4° to 24° while HI-2 observes from 19° to 89°. While their fields of view overlap they do not have full PA coverage, but instead they are circular, with the diameter on the ecliptic plane. *STEREO A* observes across a line extending to its east (left, with the Sun to the right), while *STEREO B* observes to its west (with the Sun to the left). Heliospheric imaging is a relatively new field in space physics, as the first complete heliospheric imager (SMEI) was launched less than a decade ago

(Eyles et al. 2003). It has been well established that CMEs and other solar wind structures can be tracked to large angles using heliospheric imagers. Studies involving such observations include Tappin et al. (2004), Howard et al. (2006), Harrison et al. (2008), Sheeley et al. (2008), Rouillard et al. (2008), Webb et al. (2009), Tappin & Howard (2009a), Davis et al. (2009), Möstl et al. (2010), and Sheeley & Rouillard (2010). A review of observations by heliospheric imagers can be found in Harrison et al. (2009).

In an accompanying paper, DeForest et al. (2011b) described the development of a new processing pipeline for *STEREO*/HI-2A and we use same pipeline in the present study, which has now been developed for HI-1A, COR2-A, and COR1-A. The details of how the HI-2 data are processed are described by DeForest et al. (2011b), but briefly the processing procedure undergoes five major steps: stationary background removal, celestial background removal (including cross-image distortion measurement), residual F corona removal, moving-feature filtration in the Fourier plane, and conversion back to focal plane coordinates. The result is a significantly cleaned-up sequence of images with the background stars and F corona reduced by more than three orders of magnitude.

The HI-1 data set was processed similarly to HI-2 as described by DeForest et al. (2011b), with one difference. The polynomial fit step (used to remove second-order F corona artifacts) was performed in the observing coordinate system rather than the celestial coordinate system. This was in order to overcome the far higher F coronal brightness gradients in the HI-1 field. The COR1 and COR2 data sets were processed using simple F coronal subtraction only, as the remnant K coronal signal is quite bright compared to the background star field.

Because of the large variation in intensity across the fields of view of the four instruments, it was necessary to normalize brightness across the SECCHI movie (in Figure 3). Each processed data set has an approximate zero point, so it was only necessary to apply a multiplicative correction to normalize the intensity. We divided each column (annulus in observing space) by the first quartile value of the entire data set at that elongation, i.e., the value for which 25% of all pixels are fainter and 75% are brighter. The movie is calibrated in such "quartile units" and ranges from 0 to 6. We observe that this scaling very closely approximates an r^3 radial filter.

Each of the SECCHI instruments operates with a different cadence, requiring standardization of frame times. The movie was created by sampling time at a uniform cadence of 20 minutes. For each time sample, the closest-in-time exposure (as determined from the "DATE-AVG" field in the FITS header) from each of COR1, COR2, HI-1, and HI-2 was selected to create the corresponding movie frame. Sampling in this manner is the most appropriate way to combine the differently sampled data, because it makes clear the differing cadences of the different instruments while still conveying the impression of motion to the eye.

2.2. Terminology

The flux rope component of the CME is observed at many different stages and by different observers (i.e., instruments), and historically different terms have been used to describe each observation. In the classic three-part CME the cavity component is assumed to be the flux rope, while the term "magnetic cloud" describes a phenomenon detected in situ with specific signatures as defined by Burlaga et al. (1981). These signatures do not include decreased density, although the vast

Table 1
Three-dimensional Results for Four Features Identified in the 2008 December CME

Feature	Triangulation (°)		TH Model		
	Λ	Φ	Λ	Φ	ρ
Bright front (north)	41.3 ± 35.4	-41.6 ± 10.1	24.0 ± 19.3	-12.3 ± 28.0	2.13
Bright front (south)	-4.4 ± 5.1	-31.8 ± 24.8	-9.6 ± 12.0	-8.8 ± 12.0	-0.10
Cavity (front)	50.3 ± 26.4	-38.9 ± 13.3	12.0 ± 15.5	-9.0 ± 12.0	-1.21
Cavity (back)	...	...	0.0 ± 15.8	-12.6 ± 6.0	-2.5

Notes. The four features are the northern and southern flanks of the leading bright front, and the leading and lagging edges of the cavity (void in HI-2). The latitude ($\Lambda \pm \Delta\Lambda$) and longitude ($\Phi \pm \Delta\Phi$) are given from the triangulation (COR2) and TH (HI-2) analytical results, with $\Delta\Lambda$ and $\Delta\Phi$ representing the latitude and longitude width of each feature, respectively. The ρ parameter is the distortion, which is a measurement of the concavity of each feature and is defined by Howard & Tappin (2010). Values of $\rho < -1$ indicate a concave-outward (pointed toward the Sun) structure.

majority of reported cloud observations do display a density reduction, at least when compared with the sheath region. There is no established terminology for this feature when observed by heliospheric imagers as observations of it have been rarely reported. DeForest et al. (2011b) describe it as a "void" and here we adopt this observational term. Finally, the term "flux rope" is a physical description and not an observational one. We establish in this paper that at least for one event the magnetic cloud, the coronagraph cavity and the void in the heliospheric imagers are the same thing: a flux rope originated from the lower corona. For the purposes of clarity, however, we adhere to the traditionally accepted definitions throughout the paper. That is, we refer to the in situ signature as a magnetic cloud (or simply "cloud"), the coronagraph signature as a cavity, and the heliospheric imager signature as a void. We discuss flux ropes only in their physical sense. The term "CME" refers to the complete collective structure, including the leading edge, sheath, cavity (cloud), and filament.

2.3. The Events

DeForest et al. (2011b) show HI-2A and in situ density results for 10 days from 2008 December 12 to 22, and our main study focuses on the CME observed during this time period. The December 12 CME has been studied at length and discussed in several publications. Davis et al. (2009) identified a number of features related to the CME in HI-2A, compared the predicted arrival times of these features with *ACE* in situ data, and discussed the geoeffective consequences. Liu et al. (2010) attempted triangulation with the HIs and compared an ecliptic elongation–time plot with in situ data, while Lugaz (2010) attempted three-dimensional reconstruction using the Harmonic Mean technique and compared his direction calculations with those of other methods. Finally, Byrne et al. (2010) performed a geometrical triangulation technique on the event and discussed one possibility for its physical evolution through the heliosphere. With the exception of Davis et al. (2009), the features that were identified using SECCHI in all of these studies were bright features, and the evolution of the cavity or void component has not been investigated with any depth.

The CME was launched on 2008 December 12 and a structure of increased density and speed arrived at 1 AU on December 16. A magnetic cloud was observed later on December 17, observed by *ACE* (Davis et al. 2009) and *Wind* (Liu et al. 2010). The results in this paper show that part of the cloud also passed over *STEREO B* on December 16 (see Figure 2 and related discussion). The CME was slow (transit time from 0 to 1 AU of ∼4 days) and produced no apparent forward shock. The four

studies indicate that its trajectory was almost directly at the Earth, with three separate techniques placing it within 20° of the Sun–Earth line (Lugaz 2010). Images of the CME appear in Davis et al. (2009), Liu et al. (2010), and Byrne et al. (2010) so we do not reproduce them here. Note that the COR2-B image of the CME in Figure 1 of Byrne et al. (2010) clearly shows the event as a classic three-part CME.

On 2009 January 7 and 8, two further CMEs were launched into the SECCHI-A field of view (FOV). Both of these events were directed some distance from the Sun–Earth line, so they did not impact the Earth, but we show later in this paper that one of them may have impacted *STEREO B*. No in situ information is available for the other, but we attempt to make deductions about its flux rope properties by a simple comparison with the December and other January CME observations.

2.4. Analysis

To provide us with an indication of the three-dimensional structure and direction of the three CMEs we have used geometric triangulation on the coronagraph observations (following Howard & Tappin 2008) and the Tappin–Howard (TH) model (Tappin & Howard 2009b) on the HI-2 observations. TH make use of geometry and Thomson scattering to estimate the structure, trajectory, and kinematic evolution of any feature from which a leading edge measurement can be obtained. Table 1 shows the results from these analysis techniques. We find that both techniques provide a broad agreement for the size, structure, and direction of each CME, although there was no measurable single bright front in HI-2A which required us to make separate measurements of the northern and southern flanks. Lugaz (2010) provides a variety of results for this event using different methods and our result agrees with their Fixed-Φ and Harmonic Mean results as determined using *STEREO A*. Their results show a direction of 15° east (i.e., toward the *STEREO B* direction), which is somewhat closer to the Sun–Earth line than our triangulation results, but in agreement with the TH results. The triangulation results do not indicate an impact with the Earth, but an impact is predicted by TH for two features and a miss by less than 10° for the other two. The triangulation results predict an impact with *STEREO B*'s longitude but not its latitude, and TH predict a miss of *STEREO B* by around 25° for each feature. Along with the latitude and longitude, TH also provide an additional parameter ρ which is a measurement of the concavity of the feature. This is defined by Howard & Tappin (2010) but briefly: $\rho = 0$ indicates a perfect spherical shell; $\rho > 0$ indicates a more convex structure than the shell (approaching a bubble); $\rho = -1$ indicates a flat structure (normal to the solar
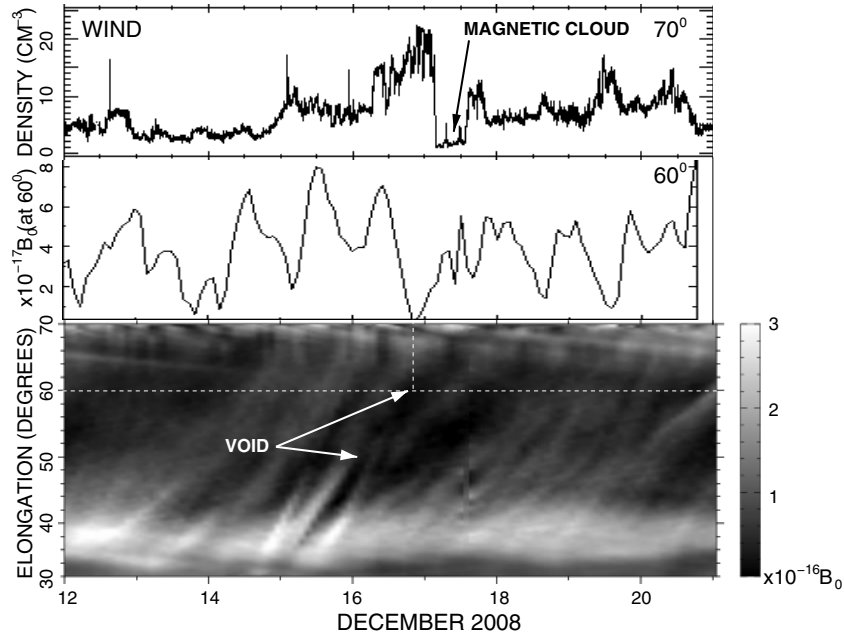
Figure 1. HI-2A observations of the 2008 December CME (spanning December 12–21) with associated in situ data. Bottom: J-map along the ecliptic from the HI-2A pipeline described by DeForest et al. (2011b). Middle: intensity–time plot of a single bin at 60° elongation (indicated by the horizontal dashed line in the J-map). Top: *Wind*/SWE solar wind density data at the location of the Earth (at 70° elongation). In all three panels, the common feature is indicated as an in situ magnetic cloud and as a void in HI-2: i.e., a region of decreased density (and intensity). This can be tracked through the J-map back to at least 35°.

radius vector), while $\rho < -1$ indicates a concave-outward (i.e., curving toward the Sun) structure. The TH results for the cavity, both for the leading (front) and lagging (back) edges, indicate a concave-outward structure.

Analysis of the magnetic cloud flux rope as observed in situ has been performed by Liu et al. (2010) and we only summarize it here. They identified a magnetic cloud using the standard signatures that also corresponded to a region of decreased density from 0400 to 1430UT on December 17, which given a bulk speed of ∼330 km s^{-1} provides a width of the cloud along the Sun–Earth line of ∼0.08 AU at 1 AU. The direction of rotation of the field is counterclockwise relative to *STEREO A*. The presence of a magnetic cloud near the Earth is confirmed independently by the results of Davis et al. (2009).

3. RESULTS

We have compared the three-dimensional reconstruction results with the timing of features as they appeared in the in situ data in order to produce a complete picture of not only the flux rope evolution of the CME, but also of the sheath region.

3.1. The Magnetic Cloud

Now that the presence of a magnetic cloud (and therefore a flux rope) is established as a region of decreased density near the Earth at 1 AU, we may identify its signature in the HI-2A data set, in which the Earth lies at ∼70° elongation. This is most easily demonstrated using a J-map, which is an elongation–time plot at a given PA obtained from a sequence of stacked images (see Davies et al. 2009 for a discussion of its implementation). DeForest et al. (2011b) provide a first attempt at the J-map of this interval along with a comparison with in situ data and a further refinement using the latest pipeline is shown in Figure 1. This figure shows the J-map (bottom), the in situ density plot from the *Wind* spacecraft (top), and the middle plot shows intensity versus time for the bin in the J-map corresponding

to 60° elongation. This J-map bin is a representation of the intensity (and therefore density) at this elongation along the ecliptic plane, but not necessarily along the Sun–Earth line. Note that a number of features that appear in the J-map bin do not appear in the in situ density plots. We interpret this to mean that the additional features occur at meridians other than the Sun–Earth line. Leaving those aside, the main features (intensity peaks and voids) appearing in the in situ density plot also appear in the binned plot, (albeit with a time lag due to the 10° difference between the bin and the location of the Earth), meaning that they also appear in the J-map. Of particular interest is the feature labeled in each plot as the in situ magnetic cloud and the HI-2 void.

A likely magnetic cloud was also observed in *STEREO B* from 08UT on December 16 until around 04UT on December 17. Its signature is shown in Figure 2. The rotation of the B-field vector, the increased B-field strength, and the reduction in temperature are the three signatures of a magnetic cloud as defined by Burlaga et al. (1981). The timing of this cloud at *STEREO B* corresponds exactly to the arrival of the void in HI-2A at 49° elongation, which is the elongation at which *STEREO B* lies at this time (relative to *STEREO A*). This shows that the magnetic cloud most likely also impacted *STEREO B*. We note that the duration of the cloud (20 hr) and its speed of around 330 km s^{-1} indicate that the cloud width at *STEREO B* (0.16 AU) is twice that at the Earth (0.08 AU). Naively, this would imply that the central axis of the cloud was closer to *STEREO B* than to the Earth, but the arrival times of the cloud at both spacecraft combined with the radial geometry of the cloud suggest that this is not the case. We therefore conclude that the fitted width of the flux rope in this case is a poor indicator of its longitudinal position relative to the observer. The longitudinal center is most likely closer to the Earth than to *STEREO B*, based on the TH model and other tracking data. This conclusion is strengthened by the observation (in Sections 3.2 and 3.3 below) that shape of the void is not consistent with the usual force-free
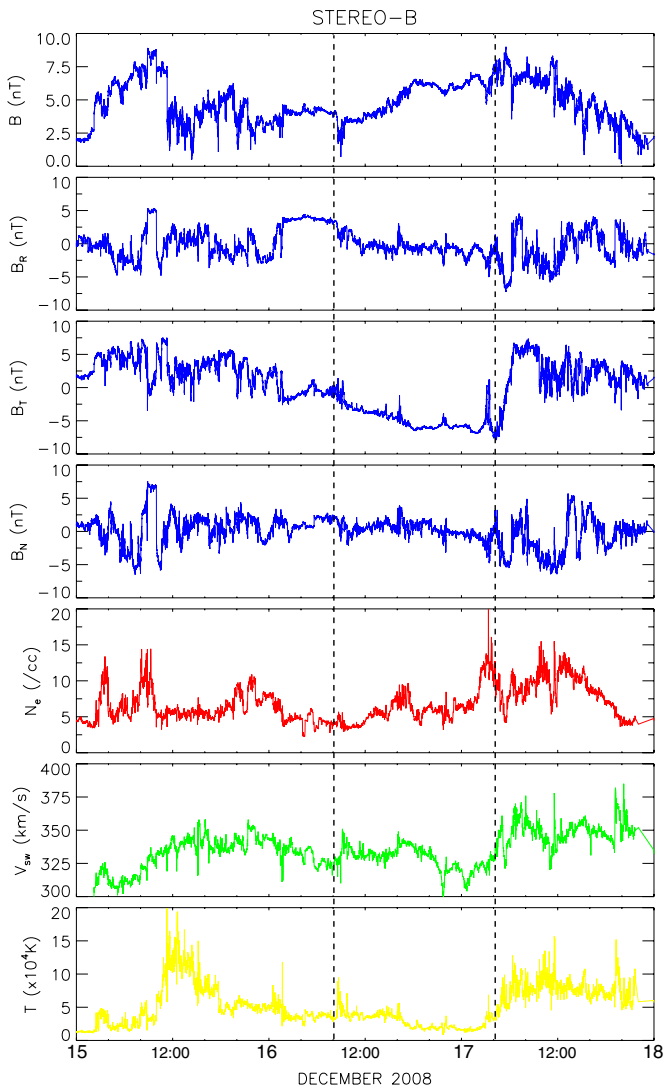
Figure 2. *STEREO B*/IMPACT and /PLASTIC in situ data from 00UT on December 15 until 00UT on December 18. In order from top to bottom are: total magnetic field strength, the radial B_R, tangential B_T and normal B_N components of the field, proton number density, bulk plasma speed, and temperature. Between around 08UT on 16 December until ∼04UT on 17 December (indicated by the vertical dashed lines), there is an apparent smooth rotation of the B field (indicated by the relatively smooth variation of the three B-field components), an increase in the field strength, and a reduction of temperature. These are the three signatures of a magnetic cloud.

(A color version of this figure is available in the online journal.)

interpretation used to extrapolate cloud structure from the in situ measurements.

3.2. Tracking the Cloud through SECCHI

Utilizing the new pipeline for the entire SECCHI imager suite (excluding the EUVI data), we may now investigate the passage of the CME from the Sun through 1 AU. Figure 3 shows frames from the movie of the CME as it passed through SECCHI-A. (The complete movie is available in the online version of this paper.) The *x*-axis is in units of degrees of elongation and is log-scaled, and the *y*-axis is the azimuth angle in heliographic coordinates in units of degrees. The transformation to this coordinate system is conformal, so that small features maintain their aspect ratio and shape. Large features are bent outward as indicated by the straight edges of each FOV, which must be used as a comparison to judge the direction of each feature's

concavity. We establish during the analysis that the distortion we measure is greater than that caused by the mapping and is therefore real. As this is from the SECCHI-A suite the Sun is located to the right with its center off the scale, and the Earth lies within the dark band at 70° elongation, near 5° azimuth. In these coordinates at this time the ecliptic plane is the line at this incline.

The CME itself first appears in the COR1-A FOV in the image on 2008 December 12 at 09UT and can be tracked almost continuously on its passage through the fields of view of all four SECCHI imagers, ending within the HI-2A FOV. (The complete HI-2 movie alone is provided by DeForest et al. 2011b.) By 14UT the complete cavity within the CME is fully visible spanning COR1-A and COR2-A and it can be tracked through HI-1A and into HI-2A, where it becomes the dark cavity that first appears in HI-2A on 12/14 at 22UT, and is fully visible by 12/15 at 08UT. The cavity region is outlined in Figure 3.

The passage of the cavity is most easily identified using a J-map of the combined SECCHI images. Figure 4 shows this map for the PA along the ecliptic line. The top portion corresponds to that in the bottom panel of Figure 1, but only extends out to December 17. The cavity that matches with the in situ cloud is labeled, and it can easily be tracked back to a dim region in COR-1A around noon on December 12. The size of this cavity is implied by the width along the *x*-axis of this region. By direct, continuous association it is clear that the cavity within the coronagraph and the void in HI-2 are the same feature, and therefore that the cavity component of this three-part CME became the in situ magnetic cloud. Similar clarity holds in all CMEs that we observed in this data set, though this is the only one where flux rope structure was clearly detected in situ.

3.3. Snowplow Pileup

Also shown in Figure 4 is a bright region ahead of the cavity. This is quite faint (but present) in COR-1A, but increases in both size and intensity as it evolves into HI-1A. When tracked through the void in HI-2A to the in situ data set, this region corresponds to a sheath region extending from around 04UT on December 16 to the start of the magnetic cloud early on December 17 (labeled "CME" in DeForest et al. 2011b). This CME did not form a foreshock or at least not one that was measurable by *Wind*. The still frames in Figure 3 and the J-map both indicate that the leading edge accumulates material as the CME propagates. This is directly visible in the J-map as a radially increasing total brightness that dominates the total brightness of the feature by the middle of the HI-1 field. It seems clear that this bright material is piled-up solar wind material ahead of the magnetic flux rope or material resulting from the so-called snowplow effect (e.g., Tappin 2006). If this is the case, then the results here demonstrate that snowplow occurs even for slow CMEs (Davis et al. 2009 provide speeds of <450 km s^{-1} for the coronagraph CME) and that material pileup occurs early in the evolution of the CME, even within the COR1 FOV (i.e., within 2 $R_\odot$).

Figure 5 shows the TH results for the leading edge of two structures corresponding to the northern and southern flanks of the bright front ahead of the void observed in HI-2A. This is a three-dimensional reconstruction of the leading edge at 00UT on December 15, when the northern flank was at a modeled distance of 1.0 AU and the southern flank was at 0.7 AU from the Sun. We were unable to obtain a complete measurement of this structure and the radial distances are different, but the
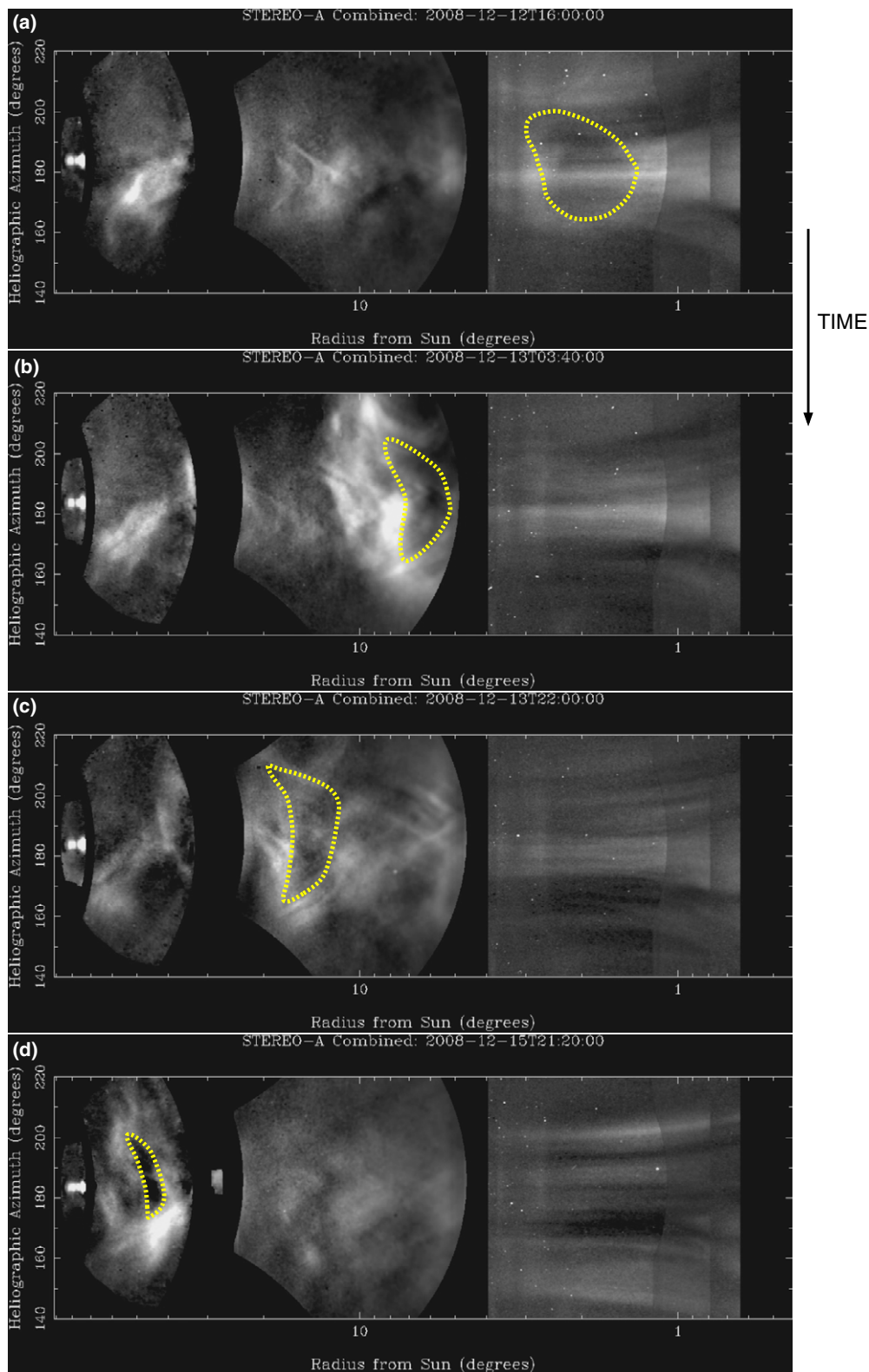
Figure 3. Selection of combined SECCHI-A frames from the movie obtained on December 12 at 16UT, December 13 at 0340UT and 22UT, and December 15 at 2120UT. The Sun is to the right at (0,180) and the Earth is at (5,70). The units on both axes are in degrees: heliographic azimuth (y-axis) and solar elongation (x-axis). The x-axis is logged. The SECCHI imagers are from right to left: COR1-A, COR2-A, HI-1A, and HI-2A. The magnetic cloud is outlined in yellow as a void that can be tracked through each imager.

(An animation and a color version of this figure are available in the online journal.)

longitudinal results are in close agreement. This observation of pileup in front of a slow CME is consistent with the recent observation by DeForest et al. (2011a) of a pileup in front of a disconnection event, and their conclusion that accretion drag is important to outflowing features even at speeds close to that of the surrounding wind.
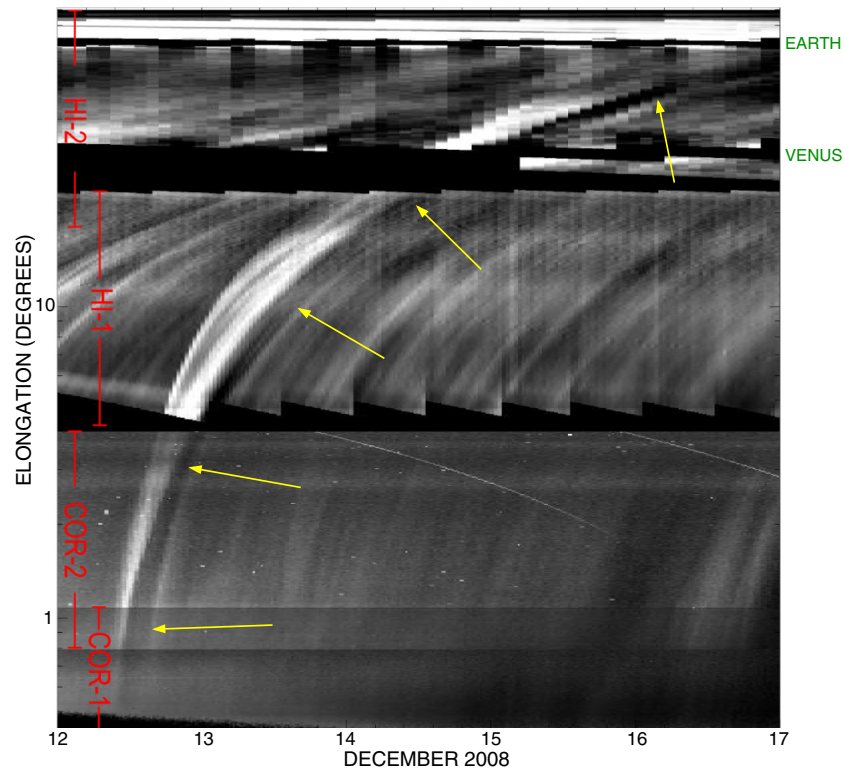
Figure 4. J-map of the data from the entire SECCHI imager suite for the CME, from December 12 to 17 with the fields of view of each imager indicated in red and the dark bands due to Earth and Venus are labeled in green. The elongation (*y*-axis) is plotted using a log scale. The magnetic cloud is the void indicated with the yellow arrows.

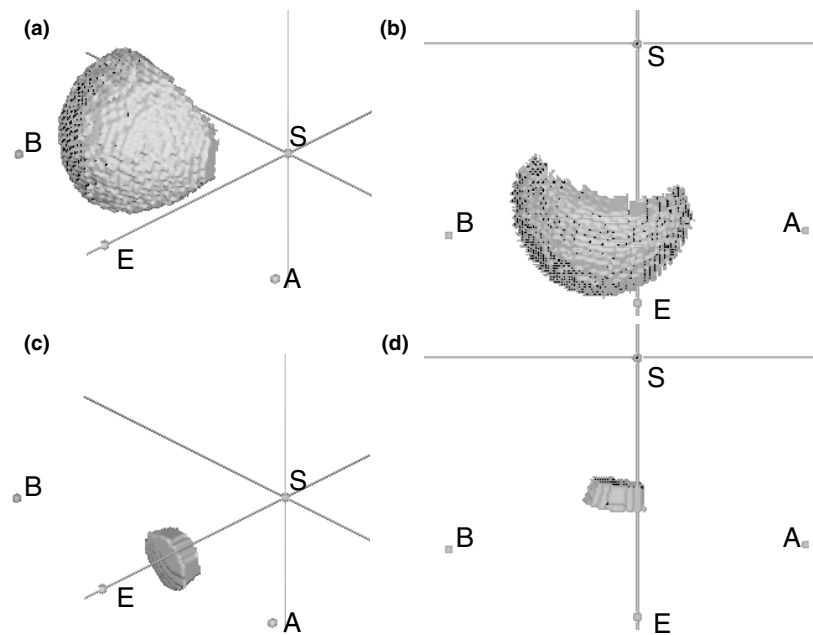(A color version of this figure is available in the online journal.)

Figure 5. TH model three-dimensional reconstructions of the leading edges of two bright structures ahead of the cavity on 2008 December 15 at 00UT. The top row (a and b) is for the northern structure and the bottom row (c and d) is for the southern structure. At this time (December 15 at 12UT) the center of the northern structure was at 1.05 AU and that of the southern structure at 0.6 AU from the Sun. Panels (a) and (c) show the structures from a viewpoint at 30°N, 45°W of the Sun–Earth line, while (b) and (d) show the views looking straight down onto the north axis of the ecliptic plane. The locations of the Sun (S), Earth (E), and both *STEREO* (A and *B*) are indicated.

3.4. Evidence of Flux Rope Distortion

Figure 3 also suggests that the structure of the void becomes distorted on evolution through the heliosphere. With the exception of a slight distortion toward the northern flank, the cavity appears almost circular in the COR1 and COR2 FOV, but even by the time it reaches the HI-1 FOV it is no longer circular and appears to be concave outward. This is seen in Figure 3 in the tighter outward curvature of the void leading edge when compared with the distorted (originally straight) edges of the
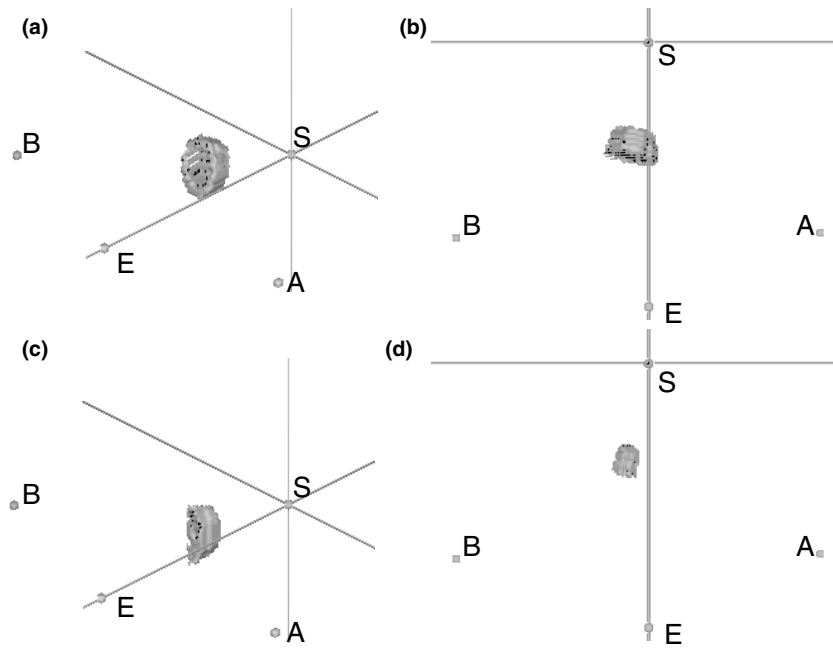
Figure 6. TH model three-dimensional reconstructions of the leading and trailing edges of the void as observed in HI-2. The top row (a and b) is for the leading edge and the bottom row (c and d) is for the trailing. These are at the same time as the features in Figure 5 (15 December at 12UT), and the center of the leading edge is at 0.45 AU with the trailing edge at 0.40 AU from the Sun. As with Figure 5, (a) and (c) show the structures from a viewpoint at 30°N, 45°W of the Sun–Earth line, while (b) and (d) show the views looking straight down onto the north axis of the ecliptic plane.

fields of view. In HI-2 it has a distinct structure, also concave outward but not symmetric about the innermost point—a slight extension to the north. Here we evaluate the possible distortion effects on the structure of the flux rope.

The apparent distortion effects are evident even when the CME has first appeared in the HI-1 FOV. The innermost part of the HI-1 FOV is at 4° (approximately 15 $R_\odot$) which is well inside the limit where projection effects begin to become apparent for average-sized CMEs (which includes the 2008 December CME). The theory of the geometry of CMEs reviewed by Howard & Tappin (2009) demonstrates that perspective and projection effects into the image plane due to the geometry of the CME do not begin to play a significant role until at least 30° or even 45° for narrower CMEs. Therefore, if the CME appears distorted within the innermost part of the HI-1 FOV then it is likely to be a real distortion. The TH results from Table 1 reveal a concave-out structure for both the leading and lagging edges of the cavity, indicating that the distortion observed in HI-2 is not a geometric illusion. These results are shown in Figure 6.

In order to estimate the variation in the distortion of the cavity, we have measured its leading edge in COR1, COR2, and HI-1. To these we have assigned a least-squares second-order polynomial fit through the leading edge measurements of Point-P distance (R) and PA. Following a technique applied to Large Angle and Spectroscopic Coronagraph (LASCO) and SMEI data by Howard et al. (2007), we may estimate the curvature of the structure by measuring its concavity, given by the second derivative of the polynomial fit $d^2R/d(\mathrm{PA})^2$.

Figure 7(a) shows a sequence of snapshots of the curvature of the leading edge of the void as it passes through the COR1-A, COR2-A, and HI-1A FOV, while Figure 7(b) shows the concavity of the second-order polynomial fit through each snapshot. This figure reveals that the structure has flattened out significantly by the time the flux rope reaches ∼0.05 AU and becomes concave outward by around 0.065 AU. This concavity gradually increases (i.e., it becomes more strongly concave

outward) as the flux rope evolves. By the time it reaches 1 AU, the overall structure of the flux rope no longer resembles the circular cavity that left the Sun. Internally, as indicated by the in situ magnetic cloud, the field lines themselves maintain some form of helical structure.

Contrast the concavity of the flux rope with that of the leading sheath discussed in the previous section. The sheath maintains its concave-inward geometry throughout the propagation of the CME (even through HI-2) while the cavity appears to be increasingly concave outward. This suggests that the amount of pileup is greater at the center of the flux rope structure than along its flanks as momentum transfer from the surrounding slower-moving wind slows down the propagation.

3.5. Comparison with Other CMEs

Figure 8 shows a J-map revealing the passage of two further CMEs that were launched around 13UT on 2009 January 7 and 2020UT on January 8 (movies of these events through SECCHI are available in the online version of this paper). Although they cross the ecliptic plane (the first event appears to barely glance it), these events were considerably separated in azimuth from the Sun–Earth line and so did not impact the Earth. While there are no CME signatures in *Wind* or *STEREO A* for either event, and no signature corresponding to the first CME, there was a possible magnetic cloud measured in situ by *STEREO B* from around noon on January 15 to around midnight on January 16. While we are not certain of this signature, it does correspond to the arrival of the void of the second CME arriving at 50° elongation (i.e., the elongation of *STEREO B* relative to *STEREO A*). The COR-2A images show that both exhibit the three-part CME structure, and the cavities of each can be tracked through the SECCHI FOV as with the 2008 December event. Even though there are no in situ data available for the first CME, we can deduce that it may have contained a flux rope by comparison with the events for which we do have information in situ. Hence,
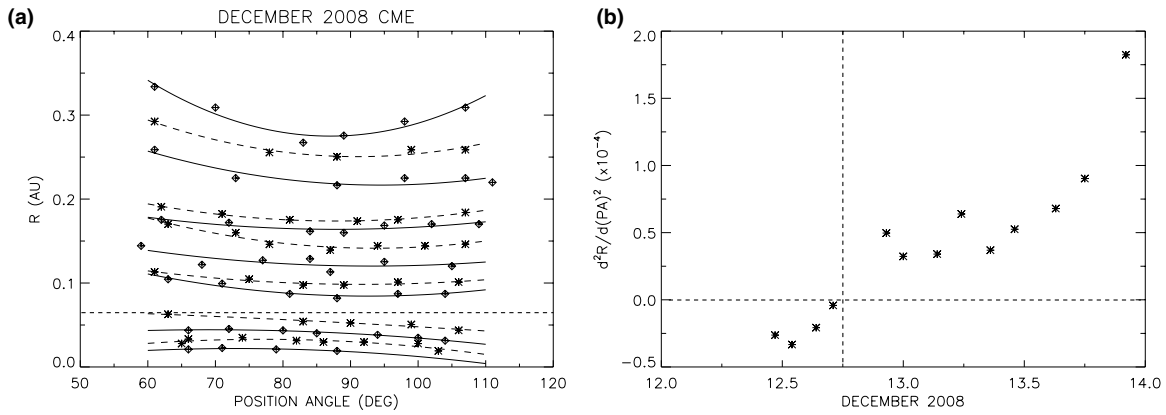
Figure 7. (a) A sequence of snapshots of an outline of the leading edge (plot of Point-P distance R vs. position angle (PA) of the void at intervals of a few hours during its passage through the SECCHI FOV (COR1-A, COR2-A, HI-1A). Elongation has been converted to units of distance (R in AU) using the Point-P approximation. The curves through the points are a least-squares second-order polynomial fit through the function of R and position angle PA. Symbols and curves have been produced with alternating designs to indicate differences between alternate measurements. (b) Plot of $d^2R/d(\mathrm{PA})^2$ of the polynomial fit showing how the concavity (i.e., curvature) changes with time. In each panel, the point of inflexion is approximated by the dashed lines. This occurs at around 18UT on December 12, when the CME was around 0.065 AU (3°7) from the Sun.
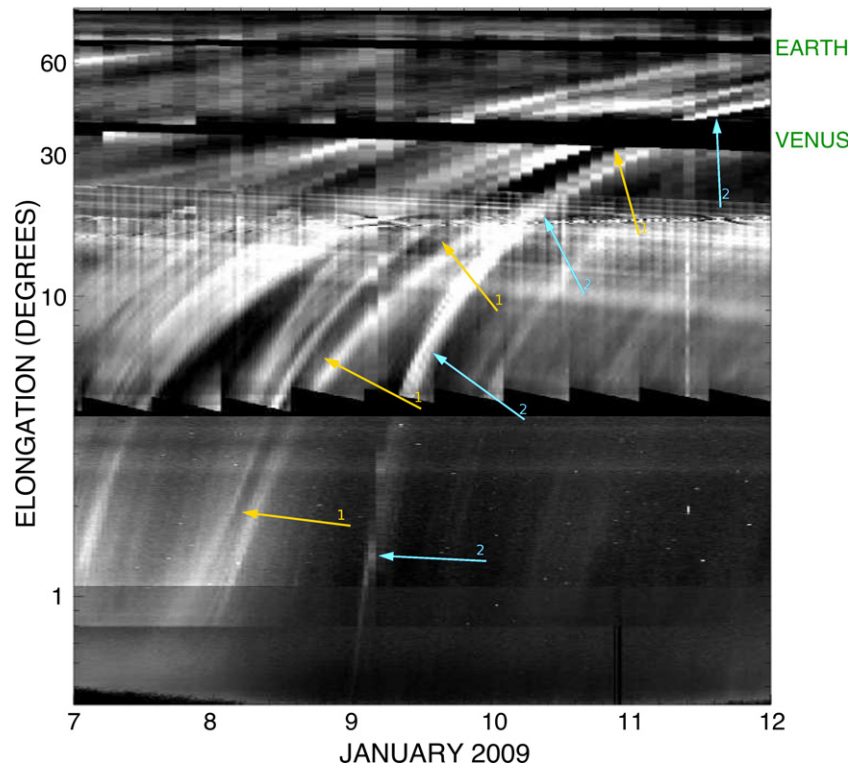

Figure 8. SECCHI J-map of the two CMEs that launched from the Sun around 13UT on 2009 January 7 and 2020UT on January 8. The movie of these two CMEs is shown in the online version of this paper. As with the 2008 December event both of these exhibit the three-part CME structure and a void can be tracked through the entire SECCHI FOV, and while the second CME does exhibit a magnetic cloud signature in situ, there are no in situ measurements for the first CME. We can deduce from the SECCHI observations, however, that these CMEs also contained flux ropes. The voids, believed to be flux ropes, are labeled by the arrows: gold for the first event, blue for the second.

(An animation and a color version of this figure is available in the online journal.)

by simple observation of events within SECCHI, we may be able to estimate whether a CME contains a flux rope and assess the extent of solar wind pileup even when there are no in situ data available for the event. While it is more difficult to track the voids through SECCHI than it was for the 2008 December event, a void is visible for both events that evolves through the HI-2 FOV, and can be tracked through the J-map in Figure 8. Here it is the void in the first event that is most easily recognized, and we conclude by simple comparison that it too may be a flux rope,

even in the absence of in situ measurements. It also seems clear that these voids also become distorted en-route, both appearing to be concave out by the time they reach the outer parts of the HI-1 FOV. While the results are not conclusive for these events, the distortions appear to begin later and are not as pronounced as with the 2008 December CME. Given that the latter two events move with a similar or slower speed than the first CME, the difference from the December CME may be because they were smaller in size.

4. MEASUREMENT LIMITS AND UNCERTAINTIES

As with all measurements of diffuse structures across very large distances there are a number of uncertainties associated with the analysis in this study. First, measurements of distance made with the coronagraphs and HI-1 have been performed using the Point-P approximation (Houminer & Hewish 1972; Howard et al. 2006). This assumes that the CME lies upon an arc of a sphere centered at the Sun (i.e., it lies in the sky plane). Given that the direction of propagation of this CME lies near the plane of the sky of *STEREO A* this is a reasonable assumption, but uncertainties are introduced due to the fact that the CME is not a single point and is not entirely confined to the sky plane.

Second, the three-dimensional direction of propagation of the CME is uncertain. Attempts at determining the direction of this event have been made by many workers (Davis et al. 2009; Liu et al. 2010; Lugaz 2010; Byrne et al. 2010) and these techniques do not all yield a common consensus. Lugaz (2010), for example, showed the results from four different techniques on several different CMEs and found little agreement for the direction of propagation. We have used two independent techniques for the bright front and found broad agreement between them, and these results were broadly in the range of Fixed-Φ and Harmonic Mean results of Lugaz (2010) (with *STEREO A* as the observer). Our results also place the CME in the same quadrant as did Davis et al. (2009) and Liu et al. (2010), but not in the same as the remaining results of Lugaz (2010) or Byrne et al. (2010). Our results suggest that the magnetic cloud impacted *STEREO B* as well, somewhat validating our three-dimensional triangulation results. Comparing the results from these many publications indicates the high level of uncertainty surrounding this determination.

Third, the TH model does not accommodate for variations in multiple parameters simultaneously. As stated earlier, while it is reasonable for a first-order approximation to assume that most of the parameters are fixed, this is almost certainly not a physically accurate description of CME evolution. There is evidence to suggest that all of the parameters estimated by TH change during the evolution of the CME. It is important to note that the TH model does not reconstruct an exact picture of the fine details of the evolution of the CME, but rather provides an estimate of the location and structure of its leading edge. Additionally, we were unable to obtain a complete measurement of the entire bright front ahead of the CME, but rather separate measurements of two fragments along the northern and southern hemisphere. While the similarity between the longitudinal results suggest that they may be two components of the same structure, this fragmentation may have a significant effect on the results obtained using TH for the structure of the bright front.

Fourth, the analysis that has been attempted on the voids has been the same as those that are applied to bright structures. This was because the analytical techniques that have been devised to investigate these structures have been intended for bright structures. There may be differences between how the eye identifies dark structures and their boundaries, and also the nature of the Thomson scattered light (or lack thereof) are different for cavities. While the TH model arrived at meaningful solutions for the direction and structure of the void, we must acknowledge a possible source of uncertainty due to the differences between bright and dark structures.

Fifth, it is important to note that *STEREO A* is only able to directly observe the latitudinal extent of the structure and we therefore can only speculate on the longitudinal extent. The TH model, for example, assumes the curvature of the structure

is symmetric, and it does not accommodate for, e.g., saddle-like structures. Additional information on this curvature could possibly be obtained from HI-2B observations, but HI-2B is out of focus compared with HI-2A (Eyles et al. 2009). A pipeline for *STEREO B* along the same lines as that for *STEREO A* is planned, but has not yet been developed.

Finally, the reader is reminded that the features observed by heliospheric imagers are optically thin, and so they observe a very large range of depths from the observer's sky plane. This is demonstrated by the in situ measurements of the magnetic cloud for the 2008 December event in the present study. The cloud is observed in situ a day earlier by *STEREO B* than by *Wind* even though *STEREO B* is further away from the Sun. Geometrically, this is probably indicative of the longitudinal concave-outward structure of the flux rope (not observed by *STEREO A*), with the central axis closer to the Earth than to *STEREO B*. However the J-map of the HI-2 data set perfectly shows the arrival of the cloud at both spacecraft. This is because *STEREO B* lies at a smaller elongation (50°) than the Earth (70°). The azimuthal extent of the cloud therefore must be embedded in the J-map. Further observational evidence of the ability of the HIs to observe large depths along the lines of sight involves corotating interaction regions. These structures are observable by SECCHI over 10 days prior to their impact with the observer (Rouillard et al. 2008; Tappin & Howard 2009a). The Sun rotates over 130° in 10 days, and the largest angle between the sky plane and the observer is only 90°. Hence, SECCHI can observe structures at least 50° from the sky plane and probably further. These observations are supported by the theory of Howard & Tappin (2009) which demonstrated that the gradient of intensity dropoff as we move away from the so-called Thomson surface is shallow. This is because the intensity of scattered light due to Thomson scattering is *minimized* on the Thomson surface, which acts to partially cancel the effects of the point along a line of sight that is closest to the Sun (where the incident light and density are maximized). The result is that it is difficult to identify the location of features observed in heliospheric imagers by inspection alone. We can attempt to address this using models such as TH, but the uncertainty still remains. Comparing the top and middle panels of Figure 1 demonstrates this uncertainty. Several additional features appear in the binned intensity time plot of Figure 1 than in the in situ data. This is most likely because the additional features do not impact the *Wind* spacecraft.

5. DISCUSSION

The new SECCHI processing pipeline has enabled us to track components of CMEs with a level of detail that until now was unobtainable at large elongations. Crucially, we have identified a cavity region connected with a magnetic cloud signature in situ and traced it back to its origins as observed by coronagraphs. Using these results for a single event observed in 2008 December we have confirmed that (for this event as least) it is the coronagraph cavity that becomes the magnetic cloud observed in situ. This confirms a long-held assumption by many workers about the three-part CME structure commonly observed in coronagraphs (e.g., Forsyth et al. 2006) and validates many models currently in use that are based on this assumption (e.g., Lugaz et al. 2005; Thernisien et al. 2006; Wood & Howard 2009).

Now that the cavity is established as the flux rope throughout, we can make deductions about the nature of the bright leading front, observationally confirmed as snowplowed solar wind

material that forms the in situ sheath region. We have found that the accumulation of material occurs early in the evolution of the CME, when it is within 2 $R_\odot$, and that the material grows in size and intensity by accreting solar wind material throughout its evolution. This, we believe, is the first time the snowplow effect has been confirmed so low in the corona, and is remarkable, given the slow speed of the CMEs. This may imply that the nature of material in the upper corona and lower solar wind may be different (slower? denser?) or that the intrinsic nature of the CME flux rope may differ from that assumed previously.

The reported observations have practical implications for CME detection and tracking as well. Each of the three events observed here displayed a void in the HIs and a magnetic cloud was identified for one event, and is likely for the second. If such a void is found to exist in a large number of events, then this is a way of identifying magnetic flux ropes in HI data without the need for auxiliary in situ observations. While we have only examined one strongly verifiable case in this initial study, the data are promising and similar, systematic analysis of a full population of events is required to explore this exciting prospect.

We have also found that the geometry of the CME flux rope component is different to that of its bright leading structure. The flux rope begins as a cavity in the CORs with a concave-inward structure but it becomes distorted early in its evolution. By the time the flux rope has reached around 11 $R_\odot$ it has already been heavily flattened out, and it becomes concave outward by the time it reaches around 14 $R_\odot$. This concavity is maintained throughout the rest of its journey to 1 AU. The leading edge of its bright leading sheath, however, maintains a concave-inward structure throughout its evolution. This suggests that the amount of material accumulated at the center of the flux rope is much greater than that accumulated along its flanks. This result is physically reasonable if one considers the analogy of a V-shaped snowplow, which will accumulate more material at its center than its edges. It also provides an explanation for why the magnetic cloud radius was larger at *STEREO B* (closer to its flank) than at *Wind* (closer to its center). Perhaps the pileup induced additional compressional forces on the flux rope at its center, resulting in it being narrower there. We note that the B-field magnitude peaks at around 7 nT in *STEREO B* and 10 nT in *Wind*. A compression of the flux rope is one explanation for the increase in magnetic flux density.

The results presented here strongly suggest that the magnetic flux rope becomes distorted en-route from the Sun to the Earth. We are only able to observe the latitudinal extent with the HIs, but auxiliary in situ measurements of the timing and thickness of the magnetic cloud at different longitudes imply a longitudinal distortion as well. The implications for this study extend to observations of CMEs by coronagraphs and heliospheric imagers, and also to magnetic cloud models, as many of them rely on the assumption that the cloud is a perfect circle. Some models (e.g., Hu & Sonnerup 2001; Romashets & Vandas 2005) allow for distortion effects within the cloud magnetic structure, but the authors have yet to model one with a concave-outward flux rope structure.

For a physical description, one possibility is that the flux rope runs into more dense material at its center, meaning that the center travels with a slower speed than its flanks (such as with the so-called ghost CME observed in the early days of LASCO; Tappin & Simnett 1997). A larger concentration of material accumulating along the central part of the CME compared with its flanks is indicative of a dense region of solar wind material, such as the streamer belt surrounding the heliospheric current sheet, being present there. If this is true then the CME magnetic structure extends beyond that of the streamer belt and crosses the current sheet, meaning that the CME is neither confined nor blocked by the belt. This interpretation further indicates that, contrary to common extrapolations, at least some CME flux ropes that have been interpreted as magnetic clouds are far from force-free at the boundary and far from circular in cross section. This would be impossible to determine in situ without a large distributed fleet of spacecraft, but is simple to observe remotely.

REFERENCES

Burlaga, L. F. 1988, J. Geophys. Res., 93, 7217
Burlaga, L. F., Sittler, E., Mariani, F., & Schwenn, R. 1981, J. Geophys. Res., 86, 6673
Byrne, J. P., Maloney, S. A., McAteer, R. T. J., Refojo, J. M., & Gallagher, P. T. 2010, Nat. Commun., 1, 74
Cane, H. V., & Richardson, I. G. 2003, J. Geophys. Res., 108, 1156
Canfield, R. C., Hudson, H. S., & McKenzie, D. E. 1999, Geophys. Res. Lett., 26, 627
Chen, J., Howard, R. A., Brueckner, G. E., et al. 1997, ApJ, 490, L191
Davies, J. A., Harrison, R. A., Rouillard, A. P., et al. 2009, Geophys. Res. Lett., 36, L02102
Davis, C. J., Davies, J. A., Lockwood, M., Rouillard, A. P., & Eyles, C. J. 2009, Geophys. Res. Lett., 36, L08102
DeForest, C. E., Howard, T. A., & McComas, D. M. 2011a, ApJ, submitted
DeForest, C. E., Howard, T. A., & Tappin, S. J. 2011b, ApJ, 738, 103
Echer, E., Alves, M. V., & Gonzalez, W. D. 2005, J. Atmos. Solar-Terr. Phys., 67, 839
Eyles, C. J., Harrison, R. A., Davis, C. J., et al. 2009, Sol. Phys., 254, 387
Eyles, C. J., Simnett, G. M., Cooke, M. P., et al. 2003, Sol. Phys., 217, 319
Fan, Y. 2005, ApJ, 630, 543
Fan, Y., & Gibson, S. E. 2003a, ApJ, 589, L105
Fan, Y., & Gibson, S. E. 2003b, ApJ, 605, 1123
Forsyth, R. J., Bothmer, V., Cid, C., et al. 2006, Space Sci Rev., 123, 383
Fuller, J., Gibson, S. E., de Toma, G., & Fan, Y. 2008, ApJ, 678, 515
Gloeckler, G., Fisk, L. A., Hefti, S., et al. 1999, Geophys. Res. Lett., 26, 157
Harrison, R. A., Davies, J. A., Rouillard, A. P., et al. 2009, Sol. Phys., 256, 219
Harrison, R. A., Davis, C. J., Eyles, C. J., et al. 2008, Sol. Phys., 247, 171
Hasegawa, H., Sonnerup, B., Dunlop, M., et al. 2004, Ann. Geophys., 22, 1251
Hidalgo, M. A., Cid, C., Medina, J., & Viñas, A. F. 2000, Sol. Phys., 194, 165
Houminer, Z., & Hewish, A. 1972, Planet. Space Sci., 20, 1703
Howard, R. A., Moses, J. D., Vourlidas, A., et al. 2008, Space Sci. Rev., 136, 67
Howard, T. A., Fry, C. D., Johnston, J. C., & Webb, D. F. 2007, ApJ, 667, 610
Howard, T. A., & Tappin, S. J. 2008, Sol. Phys., 252, 373
Howard, T. A., & Tappin, S. J. 2009, Space Sci. Rev., 147, 31
Howard, T. A., & Tappin, S. J. 2010, Space Weather, 8, S07004
Howard, T. A., Webb, D. F., Tappin, S. J., Mizuno, D. R., & Johnston, J. C. 2006, J. Geophys. Res., 111, A04105
Hu, Q., & Sonnerup, B. U. Ö 2001, Geophys. Res. Lett., 28, 467
Illing, R. M. E., & Hundhausen, A. J. 1985, J. Geophys. Res., 90, 275
Kaiser, M. L., Kucera, T. A., Davila, J. M., et al. 2008, Space Sci. Rev., 136, 5
Klein, L. W., & Burlaga, L. F. 1982, J. Geophys. Res., 87, 613
Lepping, R. P., Burlaga, L. F., & Jones, J. A. 1990, J. Geophys. Res., 95, 11957

Lepri, S. T., Zurbuchen, T. H., Fisk, L. A., et al. 2001, J. Geophys. Res., 106, 29231

Liu, J., Hu, Q., Howard, T. A., & Yurchyshyn, V. B. 2007, ApJ, 659, 758

Liu, Y., Davies, J. A., Luhmann, J. G., et al. 2010, ApJ, 710, L82

Lugaz, N. 2010, Sol. Phys., 267, 411

Lugaz, N., Manchester, W. B., IV, & Gombosi, T. I. 2005, ApJ, 634, 651

Lynch, B. J., Zurbuchen, T. H., Fisk, L. A., & Antiochos, S. K. 2003, J. Geophys. Res., 108, 1239

Martin, S. F., Livi, S. H. B., & Wang, J. 1985, Aust. J. Phys., 38, 929

Marubashi, K. 2000, Adv. Space Res., 26, 55

McKenzie, D. E., & Canfield, R. C. 2008, A&A, 481, L65

Möstl, C., Temmer, M., Rollett, T., et al. 2010, Geophys. Res. Lett., 37, L24103

Richardson, I. G., & Cain, H. V. 2004, J. Geophys. Res., 109, A09104

Riley, P., Linker, J. A., Lionello, R., et al. 2004, J. Atmos. Sol.-Terr. Phys., 66, 1321

Romashets, E. P., & Vandas, M. 2005, Adv. Space Res., 35, 2167

Rouillard, A. P., Davies, J. A., Forsyth, R. J., Hapgood, M., & Perry, C. H. 2008, Geophys. Res. Lett., 35, L10110

Sheeley, N. R., Jr., Herbst, A. D., Palatchi, C. A., et al. 2008, ApJ, 674, L109

Sheeley, N. R., Jr., & Rouillard, A. P. 2010, ApJ, 715, 300

Sturrock, P. A. 1989, Sol. Phys., 121, 387

Tappin, S. J. 2006, Sol. Phys., 233, 233

Tappin, S. J., Buffington, A., Cooke, M. P., et al. 2004, Geophys. Res. Lett., 31, L02802

Tappin, S. J., & Howard, T. A. 2009a, ApJ, 702, 862

Tappin, S. J., & Howard, T. A. 2009b, Space Sci. Rev., 147, 55

Tappin, S. J., & Simnett, G. M. 1997, in Proc. 31st ESLAB Symposium, ESTEC, Correlated Phenomena at the Sun, in the Heliosphere and in Geospace, ed. A. Wilson (ESA SP-415; Noordwijk: ESA), 117

Thernisien, A. F. R., Howard, R. A., & Vourlidas, A. 2006, ApJ, 652, 763

Török, T., & Kliem, B. 2003, A&A, 406, 1043

Török, T., & Kliem, B. 2005, ApJ, 630, L97

Tripathi, D., Bothmer, V., & Cremades, H. 2004, A&A, 422, 337

van Ballegooijen, A. A., & Martens, P. C. H. 1989, ApJ, 343, 971

Webb, D. F., Howard, T. A., Fry, C. D., et al. 2009, Sol. Phys., 256, 239

Wilson, R. M. 1990, J. Geophys. Res., 92, 215

Wood, B. E., & Howard, R. A. 2009, ApJ, 702, 901